NUMERICAL SIMULATION OF MIXED CONVECTION HEAT TRANSFER AND RESULTING ENTROPY USING TWO VIBRATING CYLINDERS INSIDE A CLOSED CAVITY FILLED WITH Cu-AL_2O_3-WATER HYBRID NANOFLUID

Rusul Abbas Alwan[1]
abc4005@mtu.edu.iq
[1]Technical Engineering College Baghdad, Middle Technical University, Baghdad, Iraq

Nabil Jamil Yasin[2]
Nabiljamil58@gmail.com
[2]Al_Amarah University College, Iraq

Hameed K. Hamzah[3]
eng.hameed.hamzah1@uobabylon.edu.iq
[3]College of Engineering, University of Babylon, Babylon, Iraq

ABSTRACT

This study investigated the effects of mixed convection heat transfer and entropy generation within a closed two-dimensional square cavity filled with a water-based hybrid nanofluid composed of ammonia and copper nanoparticles, by using Galerkin finite element method. The cavity contains two vertically oscillating cylinders as internal heat sources and cooled outer walls. The effects of Rayleigh numbers (10^3-10^5), oscillation amplitudes (0, 0.05, 0.1, 0.15), and frequencies (0.5,2, 2.5, 5, 10, 20, 40) on flow behaviour, entropy, Bejan number, and local Nusselt number were investigated. The remaining parameters, such as the volume fraction of the nanoparticles (2.5% Cu, 2.5% Al_2 O_3), the shape, position of the cylinders and the Prandtl number (6.2) were kept constant, assuming laminar flow. The results showed that the Rayleigh number was the influential factor in enhancing heat transfer and frequency, while the oscillation amplitude effect was relatively limited, providing a deeper understanding of enhancing heat exchange mechanisms in closed-loop thermal systems with moving internal sources, making them relevant for advanced engineering applications and air conditioning and refrigeration systems. The generation of maximum entropy increased by 23.3% at A=0 and 39.9% at f=40, indicating an increase in the system's non-reflectivity within the enhanced heat transfer range.

Keywords: **Hybrid nanofluid, Mixed convection, Nanofluid, Nanoparticles, Oscillatory cylinder**

NOMENCLATURE

A	Dimensionless Amplitude of oscillation	Cp	Specific heat at constant pressure

Received: December 10, 2025.
Accepted: March 29, 2026.

F	Dimensionless frequency ($f = \omega L^2 / \alpha f$)	P	Dimensionless Pressure
Nu	Nusselt number	T	Temperature
Ra	Rayleigh number ($Ra = g\beta (T_H^* - Tc^*) L^3 /m \alpha$)	TP	Period of oscillation (TP = 1/f)
Pr	Prandtl number ($Pr = m/\alpha$)	G	Gravity acceleration
Di	Diameter of the cylinder	K	Thermal conductivity
R	Radius of the cylinder	L	Length of the cavity
x, y	Cartesian coordinates	T	Dimensional time
X, Y	Dimensionless cartesian coordinates	W	Velocity of the moving grid
W_0	The length of the cylindrical heater	U	Velocity component along x-axis
$\dot{s}$	Dimensional entropy	V	Velocity component along y-axis
$\dot{S}$	Dimensionless entropy	S	Cavity sidewall length
Fri	friction	nf	Nanofluid
ω	Dimensional frequency	hnf	Hybrid nanofluids
Φ	Volume fraction	hnp	Hybrid nanoparticles
$\bar{\theta}$	Dimensionless temperature	bf	Base fluid
τ	Dimensionless time (s = taf/L2)	c	Cold
α	Thermal diffusivity	h	Hot
B	Thermal expansion coefficient	μ	Dynamic viscosity
avg	Average	ν	Kinematic viscosity
th	Thermal	*	Dimensional parameters
gen	Generation	Γ	Irreversibility factor

INTRODUCTION

Many researchers in the field of thermal engineering have conducted scientific research on convection heat transfer processes, including forced convection, natural convection, and mixed convection, within a cavity filled with a fluid such as water or air. Given the importance of convection heat transfer in numerous industrial applications, solar energy systems such as solar cells and solar water heaters, air conditioning and refrigeration systems, battery cooling systems, electronics cooling, and other fields, scientists and researchers are constantly striving to improve convection processes. This has involved introducing porous media and nanoparticles into the fluids used to enhance heat transfer.

A hybrid fluid was placed in a horizontal annular cavity between two oval cylinders. The inner surface of the annular cavity was heated to uniform temperatures, while the outer surface was cooled, resulting in a natural temperature difference. The results showed that the flow rate, natural convection heat transfer, and the entropy resulting from heat and friction increased with increasing Rayleigh number and volume fraction of the hybrid nanoparticles (Tahar Tayebi and Hakan F. Öztop 2020).The effect of cavity shape on the flow rate of a nanofluid composed of aluminum oxide and water was investigated. The results indicated that the cavity shape significantly influences the flow structure, heat transfer, Nusselt rate, and coefficient of friction by varying the applied parameters (Ch. Abdellahoum and A. Mataoui 2022). A numerical study of natural convection heat transfer

was conducted using a Cu-Al_2O_3 hybrid nanofluid placed inside a biconcave square cavity. The study showed that the total surface area for heat transfer increases with increasing empirical factors of particle shape; therefore, different nanoparticle shapes influence each other (M.A. Hanafiah et al. 2024).

Several studies have highlighted the importance of enhancing heat transfer in the presence of oscillations. This is a crucial factor in combining natural and forced convection to generate mixed convection, significantly impacting heat transfer efficiency. Some researchers have used magnetic fields to generate these oscillations. For example, a study (R. Zhang et al. 2020), (M. Ibrahim 2022) using nanofluids of varying concentrations within a cavity fixed at a 45° angle to the horizontal and subjected to an inclined magnetic flux demonstrated that increasing the Rayleigh number and decreasing the Hartmann number led to a higher average Nusselt rate and increased entropy. Heat exchange was also enhanced with increasing nanoparticle size. Furthermore, (K. Al Kalbani, M. J. Uddin 2025) conducted a numerical study investigating the effect of a horizontal magnetic field on natural convection heat transfer in a square vessel with undulating sides containing Cu nanofluid and a Cu-Al_2O_3 hybrid nanofluid. Their results indicated that increasing the undulation coefficient enhances heat flow near the walls, and that the nanofluid promotes a higher heat transfer rate than the hybrid fluid. (A. S. Abedallh et al. 2024) confirmed in his numerical study of an air-filled cavity that has a high-temperature upper wall moving reciprocating while its lower wall cools. The numerical study showed that maintaining a constant Richardson number and increasing the aspect ratio increases the Nusselt number. (A. Kh. Kareem et al. 2016) presented a numerical study of mixed convection heat transfer using a hybrid fluid composed of (Al_2O_3, CuO, SiO_2, and $2TiO_2$) inside a trapezoidal vessel with a movable lid at varying angles of rotation and tilt and different dimensions. The heat transfer rate increased with increasing nanoparticle concentration, registering the highest value when using SiO_2 -water, followed by Al_2O_3 -water, then TiO_2, and finally CuO-water. It was observed that the Nusselt number increased even more when using flexible walls compared to rigid walls of a square cavity, especially with higher Rayleigh values (Z. Gong et al. 2025).

Some also indicated that the presence of cylinders inside the cavity enhances the process, especially when they rotate or oscillate. The results are superior compared to the static state. A study of a porous square cavity containing a moving solid cylinder showed that the flow lines and Nusselt numbers increased with increasing Rayleigh and Darcy numbers, leading to improved heat transfer (A. Abdulkadhim et al. 2018). Heat transfer was further enhanced by the rotation of the cylinder within a cavity divided into two halves: the upper half containing a nanofluid and the lower half a porous layer (H.M. Elshehabey 2014). A mixed heat transfer study of two heated cylinders rotating in the center of a square vessel filled with copper nanoparticles and water showed that increasing the Richardson number reduced the Nusselt number by 13.37%, while the Nusselt number increased by 73.25% with increasing cylinder diameter and increasing nanoparticle concentration by 3.37%. The Nusselt number also increased by 75.17% at high rotation speeds (Farhan A.I. 2021). While others have suggested that the vibration of objects within cavities can further improve the Nusselt rate due to increased mixing, which in turn enhances heat exchange (B. M. Al-Srayyih et al. 2023), one study described the effect of increasing the hot wall length of a quarter-circular cavity filled with a copper-aluminum oxide/water hybrid nanofluid.During the vibration of two elliptical objects at different frequencies and

amplitudes, the lower wall was heated while the upper wall was cooled. The vertical walls provided thermal insulation. Increasing the Rayleigh number and the hot wall length led to a greater density of temperature gradient lines near the hot and cold walls. Heat generation from the hot source increased with increasing hot wall length. (S.A.M Mehryan et al, 2019) It has been proven that high frequencies improved heat exchange, and increasing the Rayleigh number improved the Nusselt rate.

Despite numerous scientific studies and research, the topic of heat transfer and its optimization under the influence of vibrating solids within a closed cavity filled with a hybrid nanofluid still requires deeper and more intensive investigation. This is especially true in closed thermal systems containing internal obstacles, where optimal utilization of these obstacles is crucial for improving system efficiency. Understanding the heat and motion tolerance of these systems is essential for designing systems from stress-resistant materials. Furthermore, this research is beneficial in chemical reactors and other applications.

CAVITY GEOMETRY

The geometrical description of the cavity in this work is presented in Fig.1. The two cylinders inside the cavity are subjected to a sinusoidal oscillatory motion and immersed in the nanofluid. The nanofluid consisting of aluminium oxide (Al_2O_3) and copper (Cu) nanoparticles in water inside the square cavity. The nanoparticles are assumed to be in dynamic and thermal equilibrium without any agglomeration or sedimentation, i.e., they are suspended and stable.

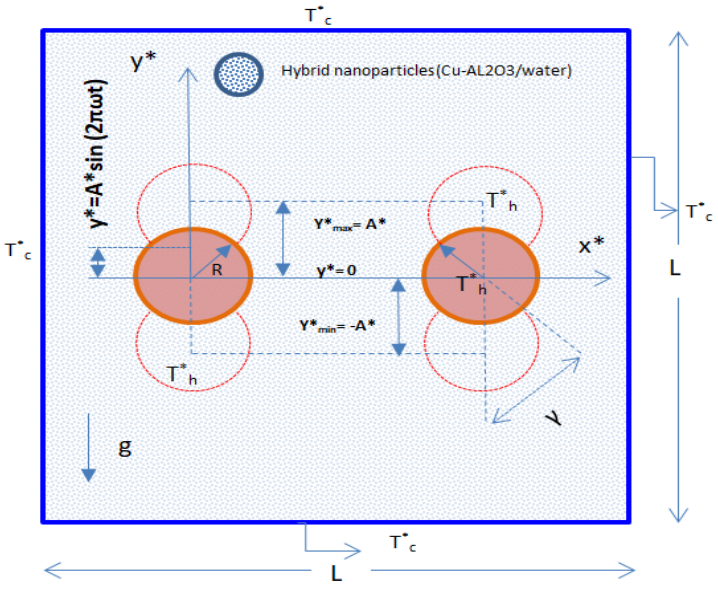

Fig. 1. Geometrical Description of the cavity.

The two oscillating cylinders oscillate along the y-axis, and their specific displacement can be defined by the equation y = A sin 2πωt, where ω is the oscillation frequency and A is the oscillation amplitude. This process involves redirecting the flow toward or away from

the hot source and generating multi-circulation fluid patterns. This, in turn, increases the heat transfer efficiency by reducing the thickness of the thermal boundary layer near the hot source wall. This increased control of heat transfer can be achieved by the motion of the oscillating solid cylinders. The thermophysical properties of the nanoparticles used in the study, as well as those of water, are given in Table 1.

Table 1. Thermophysical properties of the components of Cu–Al2O3/water (GH.R. Kefayati 2013), (H.M. Elshehabey 2014).

Physical properties	Al_2O_3	Cu	Water
c_P / J k g^{-1} K^{-1}	765	385	4179
k / W m^{-1} K^{-1}	40	401	0.613
ρ / k g m^{-3}	3970	8933	997.1
β / K^{-1}	0.85 x10^{-5}	1.67 x 10^{-5}	21 x 10^{-5}
α / m^2 s^{-1}	131.7 x 10^{-7}	1.11 x 10^{-4}	1.47 x 10^{-7}
μ /k g m^{-1} s^{-1}	-	-	8.9 x 10^{-4}

THE MATHEMATICAL MODELING

The Boussinesq approximation is applied to simulate density fluctuations at the buoyancy limit. The heat transfer equation takes into account convection and conduction from the energy equations, ignoring viscous dissipation and radiation effects. With the assumptions made above, the governing equations can be represented as follows (S.A.M Mehryan et al, 2019):

Continuity Equation:

$$\nabla^*.u^* = 0 \quad (1)$$

Momentum Equation:

$$\frac{\delta u}{\delta t} + (u^* - w^*)\nabla^*.u^* = -\left(\frac{1}{\rho_{hnf}}\right)\nabla^*.P^* + \frac{\mu_{hnf}}{\rho_{hnf}}\nabla^{*2}.u^* + \beta_{hnf}\, g\,(T^* - T_c^*) \quad (2)$$

Energy Equation:

$$\frac{\delta T^*}{\delta t} + (u^* - w^*)\,\nabla^*.T^* = \alpha_{hnf}\,\nabla^{*2}T^* \quad (3)$$

a-on all outer walls of the cavity

$$T^* \quad u=u^*=v^*=0 \quad (4\text{-a})$$

b-in the oscillating cylinder

$$T^*=T_h^* \quad (4\text{-b})$$

$$u^*= 0, v^*= dy^*/dt = 2\,A^*\pi\,\omega\cos(2\pi\omega) \quad (4\text{-c})$$

$$\frac{t\,\alpha_f}{L^2} = \tau, \qquad \frac{x^*}{L} = x \qquad \frac{y^*}{L} = y$$

$$\frac{(L^2)}{(\rho_f\,\alpha_f^2)}.P^* = P \qquad \frac{u^*\,L}{\alpha_f} = u \qquad \frac{w^*\,L}{\alpha_f} = w$$

$$\frac{\nu_f}{\alpha_f} = Pr \qquad \frac{\nabla^*}{1/L} = \nabla$$

$$\frac{\nabla^{*2}}{1/L^2} = \nabla^2 \qquad \frac{(g\,\beta\,(T_h^* - T_c^*)\,L^3)}{(\nu_f\alpha_f)} = Ra \qquad \frac{(T^* - T_c^*)}{(T_h^* - T_c^*)} = T \quad (5)$$

Non-dimensional equations (S.A.M Mehryan et al, 2019)
Based on the nondimensional parameters presented above, eqns, 1, 2, and 3 can be written as:

$$\nabla.u=0 \quad (6)$$

$$\frac{\partial u}{\partial \tau} + (u - w)\cdot\nabla u = -\left(\frac{\rho_f}{\rho_{hnf}}\right)\nabla p + \left(\frac{\rho_f}{\rho_{hnf}}\right)\left(\frac{\mu_{hnf}}{\mu_f}\right) Pr\,\nabla^2 u + \left[\frac{(\rho\beta)_{hnf}}{(\rho_{hnf}\,\beta_f)}\right] Pr\,Ra\,T \quad (7)$$

$$\partial T/\partial\tau + (u - w)\cdot\nabla T = (\alpha_{hnf}/\alpha_f)\,\nabla^2 T \quad (8)$$

In equation (7), Pr is the Prandtl number and Ra is the Rayleigh number, and equation (8) $\alpha_{hnf} = k_{hnf}/(\rho\,cp)_{hnf}$, $(\rho C_p)_{hnf}$ It is the specific heat capacity of the hybrid fluid.

$$\rho_{hnf} = \rho_f\,(1 - \omega_{hnp}) + (\rho.\,\omega)_{Al2O3} + (\rho.\,\omega)_{Cu} \quad (9)$$

$$(\rho\beta)_{hnf} = (1 - \omega_{hnp})(\rho\beta)_f + (\omega.\rho\beta)_{Al2O3} + (\omega.\rho\beta)_{Cu} \quad (10)$$

$$(\rho C_p)_{hnf} = (1 - \varphi_{hnp})(\rho C_p)_f + (\varphi.\rho C_p)_{Al2O3} + (\varphi\rho C_p)_{Cu} \quad (11)$$

Whereas $\varphi_{hnp} = \varphi_{Al2O3} + \varphi_{Cu}$

ρ_{hnf} Effective density is a property of nanofluids. and ρ_{bhnf} coefficient of thermal expansion (17)., as well as Thermal diffusivity of the hybrid nanofluid α_{hnf} The following modified

relationships were also obtained using the classical Maxwell (Maxwell JC.1881) and Brugman (S.M.S Murshed 2005**)** models to define the thermal conductivity of the hybrid nanofluid:

$$\frac{k_{hnf}}{k_f} = \frac{[khnp+2kf-2\,\omega\, hnp(kf-khnp)]}{[khnp+2kf+\omega\, hnp(kf-khnp)]} \quad (12)$$

Brugman's model (Maxwell JC, 1881)

$$k_{hnf} = (\tfrac{1}{4})[(3\omega_{hnp}-1)k_{hnp} + (2-3\omega_{hnp})k_f] + (\tfrac{k_f}{4})\sqrt{\Delta} \quad (13)$$

$$\Delta = [(3\,\omega_{hnp}-1)^2 (\frac{(k_{hnp}}{k_f}) + (2-3\,\omega_{hnp})^2 + 2\,(2+9\,\omega_{hnp}-9\omega^2_{hnp})\,(\frac{(k_{hnp}}{k_f})] \quad (14)$$

$$\text{Whereas } (k\varphi)_{hnp} = (k\varphi)_{Al_2O_3} + (k\varphi)_{Cu} \quad (15)$$

It is important to note that since the volume fraction of copper is zero, all equations and relationships used for the Cu-Al_2O_3/water hybrid nanofluid are valid. In the equations above for the Cu-Al_2O_3/water hybrid nanofluid, the thermal conductivity values and the experimental values are provided by (Rashad A. et al. 2018). The solution is completed based on the experimental values of the thermal conductivity of the hybrid nanofluid, as the relationships provided by Maxwell and Brugman cannot accurately estimate the thermal conductivity values for the Cu-Al_2O_3/water hybrid nanofluid. To obtain the viscosity of the Cu-Al_2O_3/water hybrid nanofluid, the accuracy of the classical models used is examined as follows:

Classical Models

Einstein's Model (Einstein A1956)

$$\frac{\mu_{hnf}}{\mu_f} = (1 + k_{\mu 1}{}^{*}\,\omega_{hnp}) \quad (16)$$

$$T = 0, v = u = 0 \quad (17\text{-a})$$

Oscillating cylinder (Temperature)

$$T = 1 \tag{17-b}$$

oscillating cylinder (Motion)

$$u = 0\,; \quad v = \frac{dy}{dt} = 2A\pi f \cdot \cos(2\pi f\tau)\,; \quad A = \frac{A^*}{L} \tag{17-c}$$

$$Nu_{local} = -\left(\frac{k\_hnf}{k\_f}\right) \cdot \left(\frac{\partial T}{\partial n}\right)_{\tau} \tag{18}$$

$$Nu_{avg} = \left(\frac{1}{W_0}\right)\int_0^{W_0} Nu_{local}\, ds \tag{19}$$

$$\boldsymbol{T_{avg}} = \frac{\left(\int_{\bar{v}} \mathbf{T_{local}}\, \mathbf{d\bar{v}}\right)}{\left(\int_{\bar{v}} \boldsymbol{d\bar{v}}\right)} \tag{20}$$

Where W_0 = length of the hot cylinder.

The fluid flow motion expressed as ψ is described as:

$$u = \frac{\partial \psi}{\partial y}; \quad v = -\frac{\partial \psi}{\partial x} \tag{21}$$

The following equations represent the entropy generated due to heat and frictional irreversibility ($\dot{s}_t$, $\dot{s}_{(fri)}$), which are the two factors that contribute to the generation of local entropy $\dot{s}_{gen}$ inside the cavity (M. Ghalambaz et al. 2021):

$$\dot{s}_{th} = \frac{k_{hnf}}{T^2{}_0\ [\,(\partial T/\partial x)^2 + (\partial T/\partial y)^2\,]} \tag{22}$$

$$\dot{s}_{(fri)} = \frac{\mu_{(hnf)}}{T_0\,[2\left(\frac{\partial U}{\partial x}\right)^2 + 2(\frac{\partial V}{\partial y})^2 + (\frac{\partial U}{\partial y} + \frac{\partial V}{\partial x})^2]} \tag{23}$$

$$\dot{s}_{gen} = \dot{s}_{th} + \dot{s}_{(fri)} \tag{24}$$

$$\dot{s}_{gen} = \frac{k_{hnf}}{T^2{}_0[\,(\frac{\partial T}{\partial x})^2 + (\frac{\partial T}{\partial y})^2\,]} + \frac{\mu_{(hnf)}}{T^2{}_0\{\,[2(\frac{\partial U}{\partial x})^2 + 2(\frac{\partial V}{\partial y})^2 + (\frac{\partial U}{\partial y} + \frac{\partial V}{\partial x})^2]\}} \tag{25}$$

When $T_0 = \frac{(T_h^* - T_c^*)}{2}$

$$\dot{S}_{gen} = \frac{\dot{s}_{gen} \cdot T^2_{(0)} \cdot s^2}{(k_{(bf)} \cdot [(T_h^* - T_c^*)^2])} \quad (26)$$

$$\dot{S}_{gen} = \dot{S}_{th} + \dot{S}_{(fri)} \quad (27)$$

$$\dot{S}_{th} = (\frac{k_{hnf}}{k_{bf}}) [(\frac{\partial \theta}{\partial X})^2 + (\frac{\partial \theta}{\partial Y})^2] \quad (28)$$

$$\dot{S}_{(fri)} = \Gamma [2(\frac{\partial U}{\partial X})^2 + 2(\frac{\partial V}{\partial Y})^2 + (\frac{\partial U}{\partial Y} + \frac{\partial V}{\partial X})^2] \quad (29)$$

$$\dot{S}_{gen} = [(\frac{\partial \theta}{\partial X})^2 + (\frac{\partial \theta}{\partial Y})^2] + [2 \left(\frac{\partial U}{\partial X}\right)^2 + 2(\frac{\partial V}{\partial Y})^2 + (\frac{\partial U}{\partial Y} + \frac{\partial V}{\partial X})^2] \quad (30)$$

$$\Gamma = T_0 \frac{\mu_{bf}}{k_{bf}} [\frac{s}{(\nu_{(bf)} (T_h^* - T_c^*))}]^2 \quad (31)$$

Across all the computing domains, the total $\dot{S}_{gen}$ in the dimensionless form is obtained by integrating equation (26). The Bejan number demonstrates the degree of irreversibility brought on by the formation of entropy during heat transport as: $Be = S_t / S_T$.

Mesh Validation

An irregular triangular mesh was generated as shown in Figure 2.

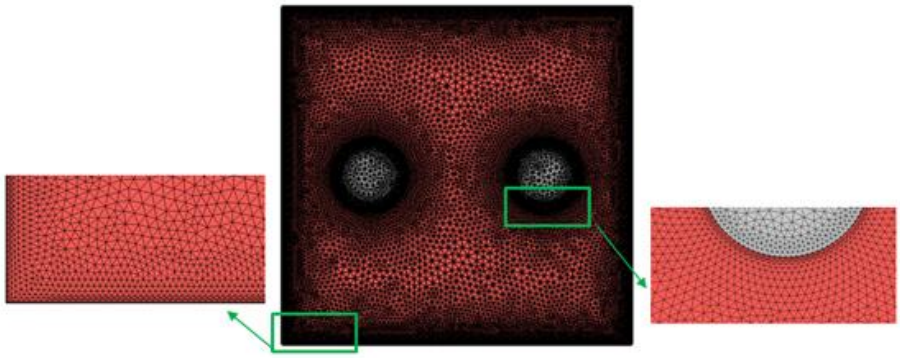

Fig. 2. An irregular triangular network showing sharp gradients in temperature and speed.

To record steep temperature and velocity gradients, a suitable number of elements were concentrated near the perimeter of the cylinder and near its walls. Initially, a basic grid of 2406 elements were constructed, and the independence of the grid was systematically studied as the number of grids increased. To ensure the independence of the results from the number of grid elements, five different grid sizes were considered. Each grid size and its resulting Nusselt number are shown in Table 2. The difference in the Nusselt number value for each grid size is also shown. It was observed that as the grid was further optimized

from 3472 to 7928, the computational effort decreased by approximately 128.3%. Table (2). Average Nusselt number for each mesh size.

Table 2. Grid independent test average Nusselt number on left cylinder surface at (φ_1=0.025, φ_2=0.025 =φ=0.0 5,τ=2, fr=5 1/sec, A=0.1) two cylinder move to up and down.

Grid	Domain elements	Boundary elements	Time min	Nu_{ave}	$\lvert Error \rvert$%
G1	2406	164	60	4.4231	-
G2	3472	200	67	4.9962	11.4
G3	7928	404	77	5.1212	2.44
G4	23494	792	124	5.1260	0.09
G5	30020	892	154	5.1270	0.019

1- The streamlines and isotherms results were compared with those published for Rayleigh equals 10^4 and 10^6. A good agreement in temperature values was observed. Furthermore, the average Nusselt number distribution, friction factor, pumping power, and thermal resistance were identified and compared as well. The validation with (M.H.M. Hashim et al 2023) was achieved at $\varphi h\, nf$ = 0.01 and ϕ = 5°.

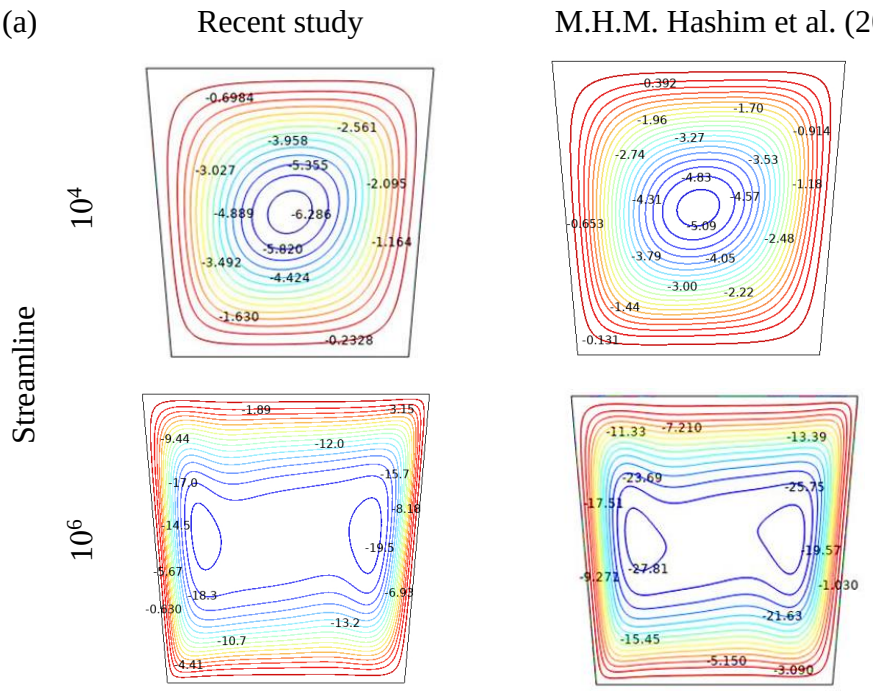

b) Recent study M.H.M. Hashim et al. (2023)

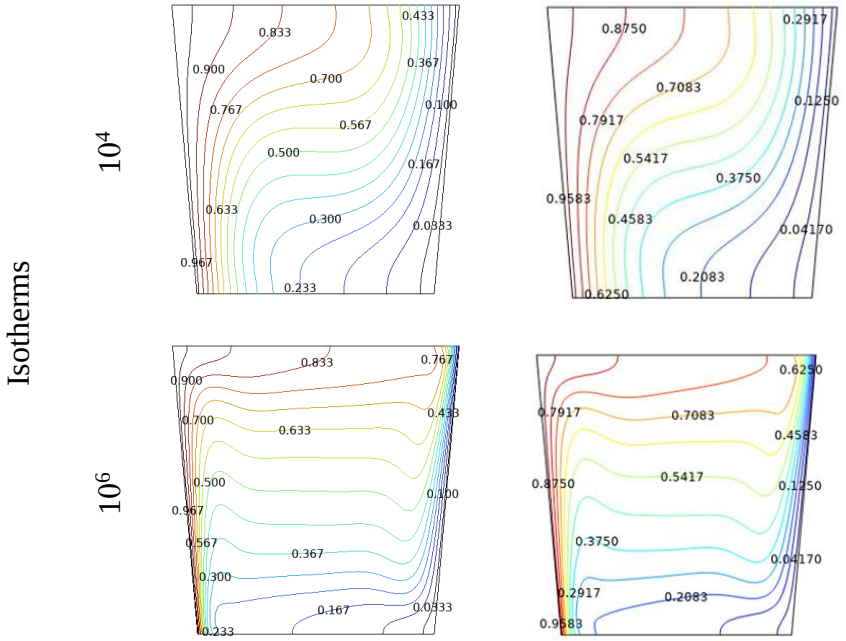

Fig. 3. (a) Flow lines, (b) Isotherms.

2- The results were compared using the COMSOL 2.6 software with published results by (D. Dey and S. K. Dash, 2023), which were simulated using Matlab b2016R software, to study natural convection heat transfer within a square cavity using ferro-hydraulic nanofluids (magnetic and non-magnetic). The comparison showed very good agreement at a concentration of φ=0.1%.

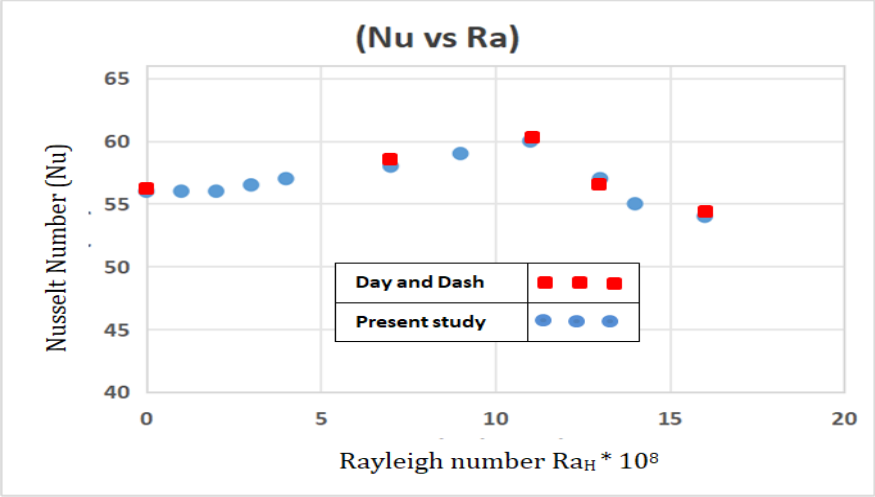

Fig. 4. Nusselt vs. Rayleigh.

RESULTS AND DISCUSSION

This section explains the simulation results for the current problem. The results are conducted for the non-dimensional cylinder parameters; Rayleigh number (10^3, 10^5), oscillation amplitude (0, 0.05, 0.1, 0.15), and frequency (0.5, 2, 2.5, 5, 10, 20, 40), with the Prandtl number fixed at Pr = 6.2. They also examine their influence on the flow and heat transfer properties.

Stream Function

Figure 5 illustrates the fluid flow function within the cavity due to the oscillatory motion of the horizontal cylinders at different values of Ra, amplitude, and frequency. The results show that, as a result of the vertical vibration of the heated cylinders within the cavity due to the oscillatory motion, vortices cover a large portion of the cavity. The vortices around the cylinder on the right side of the cavity rotate clockwise, while their direction around the cylinder on the left side of the cavity is counterclockwise. As the number of vortices increases, the flow becomes more complex, and the lines begin to curve more due to the turbulent flow. Increased line density indicates an increase in velocity. The shift of the vortices from the center to the edges indicates an increased effect of vibrations and natural convection within the cavity. Furthermore, it was observed that as the Rayleigh number increased from 10^3 to 10^5 at a constant oscillatory amplitude (Figure 5a) and a constant frequency (Figure 5b), the number of vortices generated around the heated cylinders increased. This behavior indicates turbulent flow within the cavity. Vortices are also generated in the center of the upper cavity and rotate in the opposite direction to the adjacent vortices.

It is observed that the flow velocity increases at the center and along the cavity walls for both variations in cylinder frequencies and amplitudes. Notably, at Rayleigh 10^3, new, smaller vortices are generated between the cylinders, evolving in the opposite direction to the larger vortices. The size of these vortices increases with increasing amplitude but remains smaller than the larger vortices. With increasing frequency, the smaller vortices generated become larger than the larger ones. This indicates that the flow becomes more turbulent, which in turn leads to increased heat transfer. The behavior around the two cylinders is also asymmetrical in all velocity diagrams. With increasing Rayleigh frequencies (Ra = 10^5), the flow becomes more complex and turbulent due to the presence of numerous vortices. The shape of the vortex's changes with increasing amplitude, particularly at the center of the upper cavity. The behavior also changes progressively and significantly with increasing frequency, especially at frequencies of 20 and 40.

Entropy Generation

Figures 6a and 6b illustrate the minimum and maximum entropy values and their positions at different Rayleigh numbers for constant frequency and amplitude, respectively. Generally, the highest entropy value is observed on the sides of the heated cylinder surface near the cavity walls. The lowest entropy value is found near the walls at the top and bottom

of the cavity. The comparison will be based on the highest entropy value for all cases studied in this work. Furthermore, the entropy value increases with increasing Rayleigh number from 10^3 to 10^5 . With increasing oscillation amplitude, the entropy at 10^3 Rayleigh increases very slightly. However, the behaviour at Ra = 10^5 is different. Entropy increases with smaller values of slight increases in oscillation amplitude and then decreases with higher values of oscillation amplitude (A = 0.1, A = 0.15). Entropy increases with constant Ra and increasing frequency, but at a small rate.

Bejan Number

Figures 7a and 7b illustrate the values of the Bejan number at different Rayleigh numbers for a fixed frequency and amplitude, respectively. Generally, as the Rayleigh value increases for a given oscillation amplitude (as shown in Fig. 7a) and a given frequency constant (as shown in Fig. 7b), the Bejan number decreases significantly. For the same Rayleigh value (Ra = 10^3), it is observed that with increasing oscillation amplitude and frequency (as shown in Fig. 7a and 7b, respectively), the Bejan number decreases slightly. However, at higher Rayleigh values (Ra = 10^5), the Bejan number increases with increasing oscillation amplitude. For Rayleigh 10^5 , the Bejan number increases slightly up to a frequency of 10 and then decreases down to a frequency of 40.

Local Nusselt Number

Figures 8 and 9, respectively, illustrate the trends in Nusselt numbers along the left wall for different amplitudes and frequencies. For different amplitudes at Rayleigh 10^3, the difference in Nusselt values resulting from changes in oscillation amplitudes is very small. Furthermore, the Nusselt values are identical for both cylinders. Intersecting points are observed at Rayleigh 10^3, where the behaviour is reversed. The local Nusselt value for high frequencies or amplitudes is at its lowest, while for low frequencies it is at its highest. However, the difference in values is very small. The opposite is also true. In solid A. on the left, the Nusselt value is initially high and then decreases for all oscillation amplitudes and frequencies until it reaches a point where it is low. Then the local Nusselt value increases again. In solid B on the right, the cycle starts increasing and then decreases after reaching the equilibrium point.

In Rayleigh 10^5, for different oscillation amplitudes and frequencies, the flow is more complex. At the starting point on the surface, indicated by the red circle shown in the figures, the Nusselt number values are higher than those in Rayleigh 10^3. However, they fluctuate again for several points, giving a more random appearance.

Fig. 8 shows the Nusselt number values for the two solids (A and B). Solid A has equal Nusselt values at the beginning of its cycle, while solid cylinder B has nearly equal values in the middle, indicating symmetry in flow and heat transfer due to forced convection dominating the natural flow. In Rayleigh 10^5, the flow becomes more complex due to the dominance of natural convection. The differences between the cylinders become greater,

and the Nusselt number increases significantly. This indicates that the flow of the nanofluid becomes stronger, thus increasing the efficiency of heat transfer. In solid A, the differences in the Nusselt number values were very small compared to those in solid cylinder B.

There were also several points where the Nusselt values for solid A matched. Fig. 9 shows that at different frequencies of Rayleigh 10^3, the differences in local Nusselt numbers were small, but larger than they were for different oscillation amplitudes. In Rayleigh 10^5, the flow became more complex, and the differences between the Nusselt values for different frequencies increased significantly. The highest local Nusselt number values in this case were recorded for cylinder A (6.8) at (s=0.353) and for cylinder B (6.6) at (s=0.59) at different oscillation amplitudes in Rayleigh 10^5. The highest local Nusselt number value (7.3) was also recorded in Rayleigh 10^5 for different frequency values for cylinder A at (s=0.59) and for cylinder B at (s=0.35).

CONCLUSIONS

1. Rayleigh Number Effect: The strongest factor affecting entropy and heat transfer, as Ra increases from 10^3 to 10^5.
2. The generated entropy increases significantly, and the local Nusselt number also increases noticeably, this is due to the dominance of natural convection and the increased flow intensity resulting from buoyancy forces.
3. Oscillation Amplitude (A) Effect: Its effect is very weak compared to Rayleigh number and frequency, as observed at high Rayleigh numbers, large oscillation amplitudes reduce entropy due to the dominance of convection.
4. Frequency (f) Effect: Its effect is greater than that of amplitude but less than that of Rayleigh number. It has been observed that increasing the frequency leads to a slight increase in the generated entropy and a significant increase in the local Nusselt number. This is because increasing the fluid velocity results in better mixing, which improves heat transfer through mixed convection.
5. The generation of maximum entropy increased by 23.3% at A=0 and 39.9% at f=40, This indicates that the higher frequency leads to an increase in the speed of the hybrid nanofluid movement and the shear force within the cavity, which enhances thermal mixing and increases thermal and frictional gradients, thus raising the entropy generation rates at high Rayleigh values.

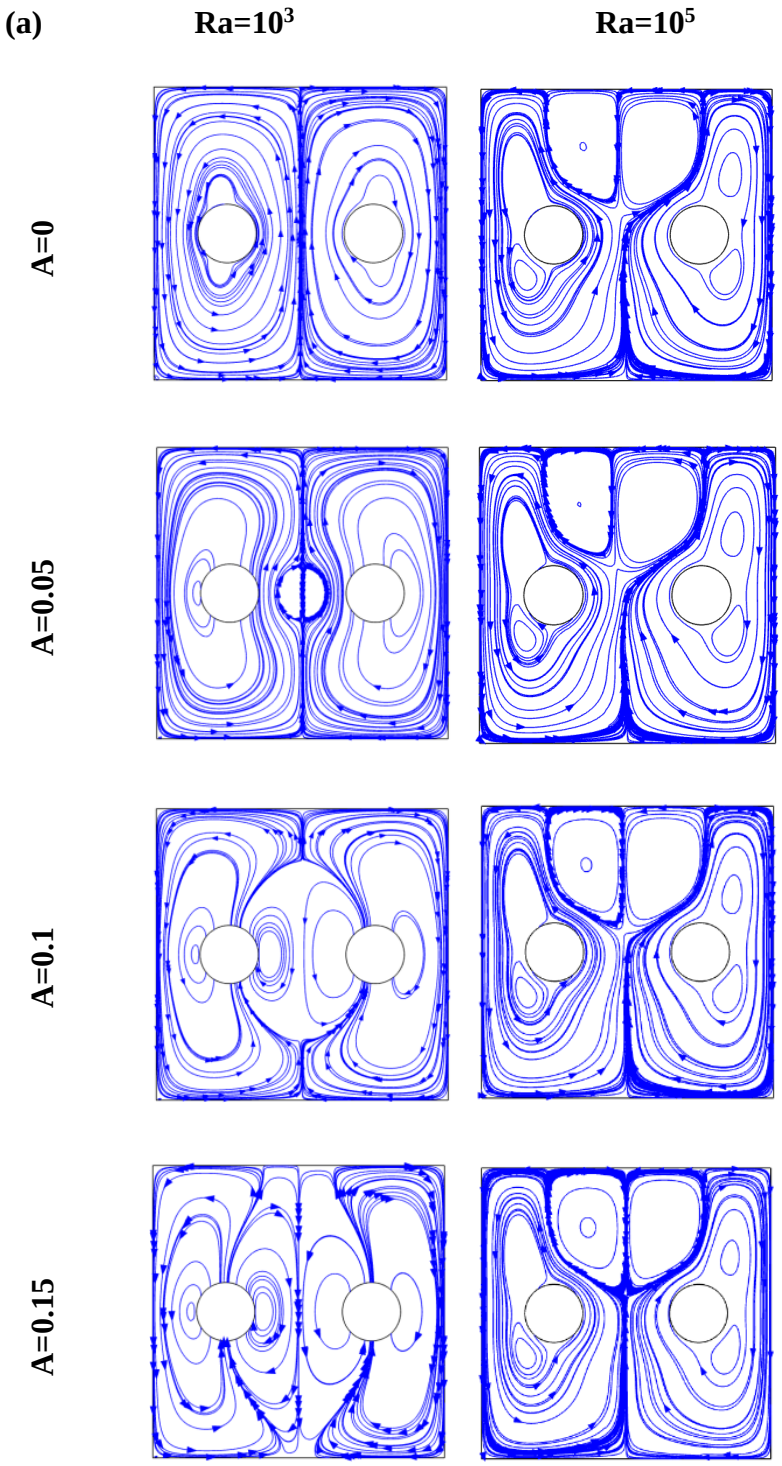
(a)
Ra=10^3
Ra=10^5
A=0
A=0.05
A=0.1
A=0.15

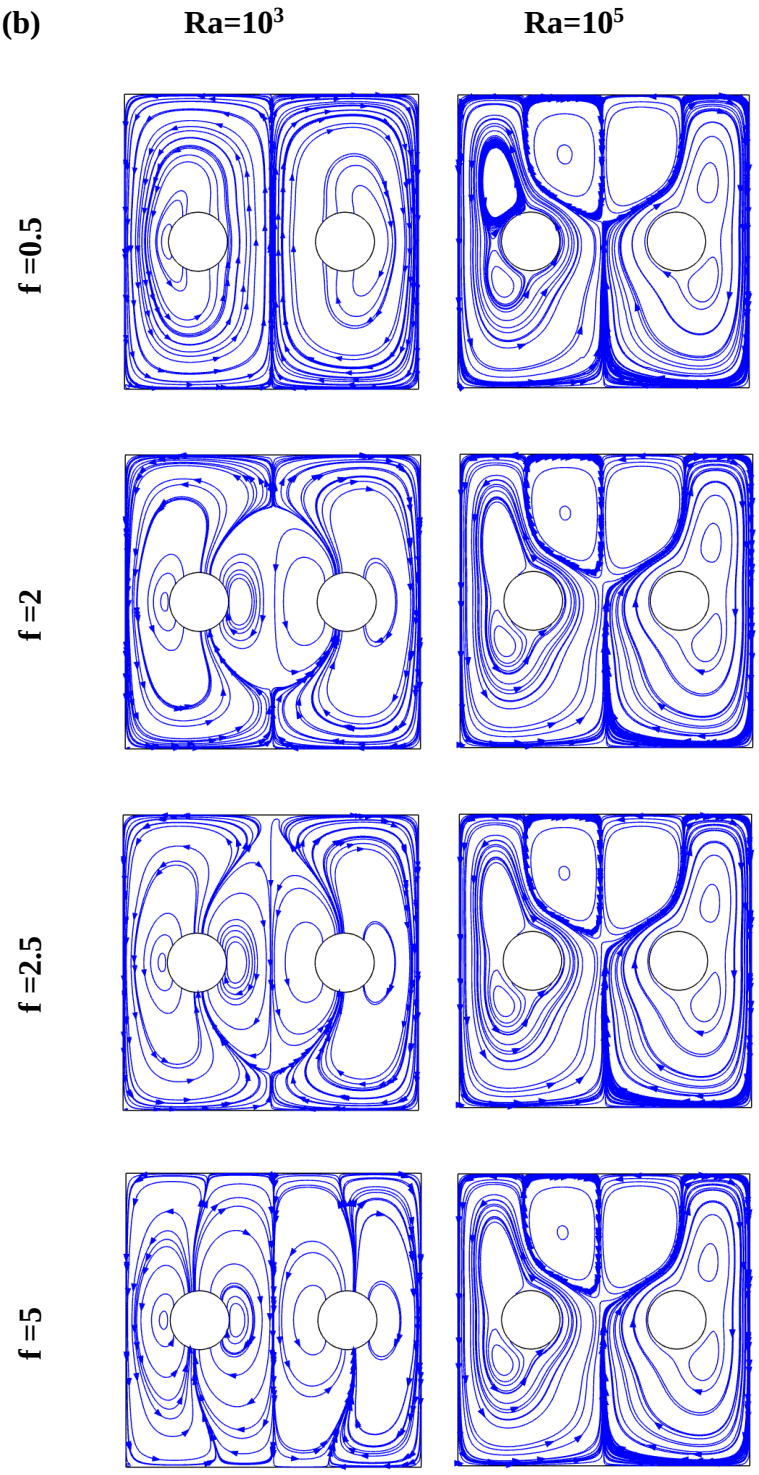
(b)
Ra=10^3
Ra=10^5
f =0.5
f =2
f =2.5
f =5

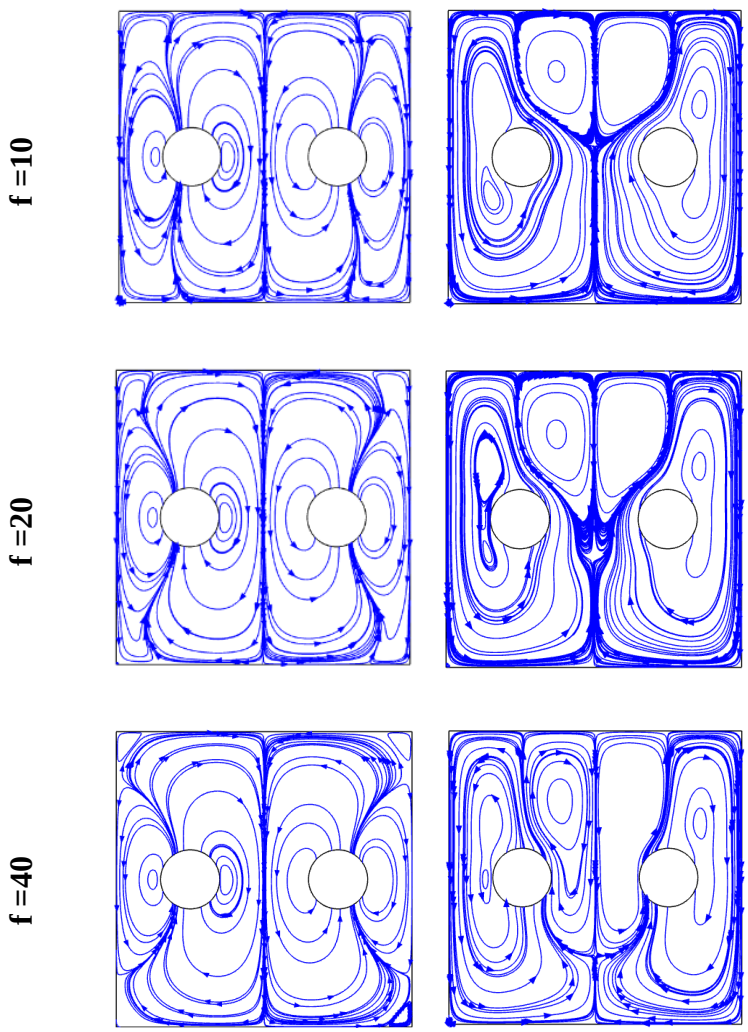

Fig. 5. Velocity and direction chart at Ra= 10^3, and 10^5, Di = 2, τ = 2, φ_{hpn}= 0.5. a) f =2; b) A =0.1.

(a) **$Ra=10^3$** **$Ra=10^5$**

A=0

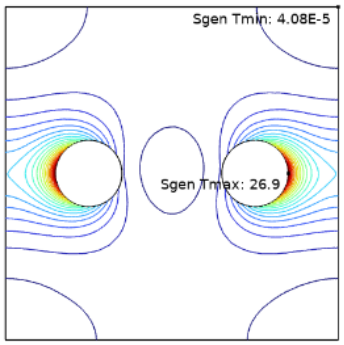

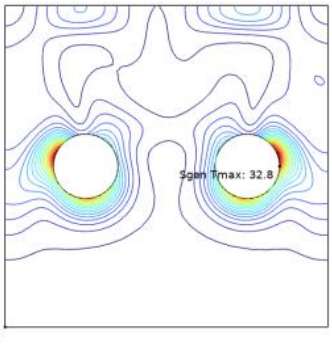

A=0.05

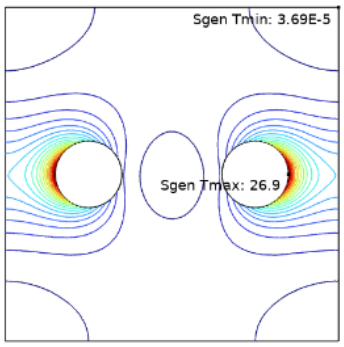

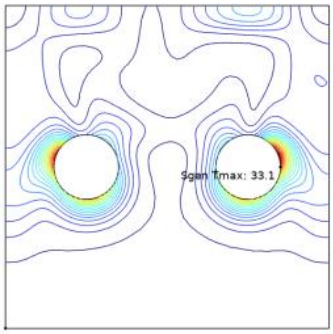

A=0.1

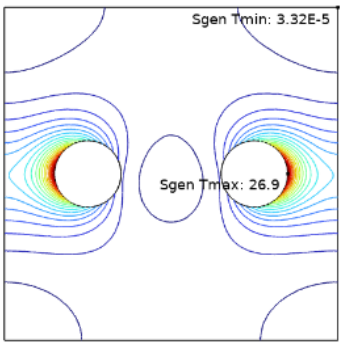

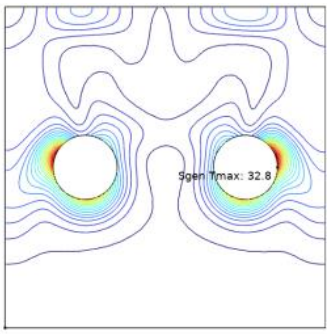

A=0.15

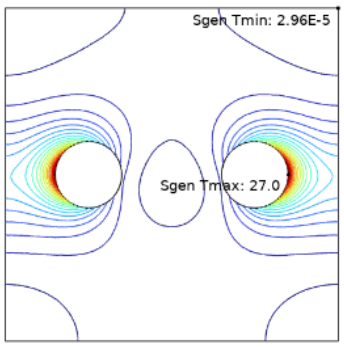

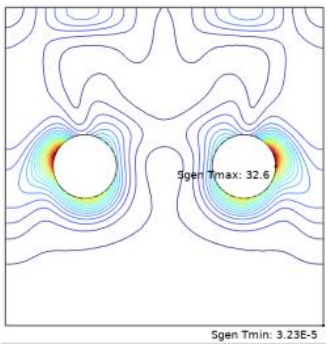

(b)

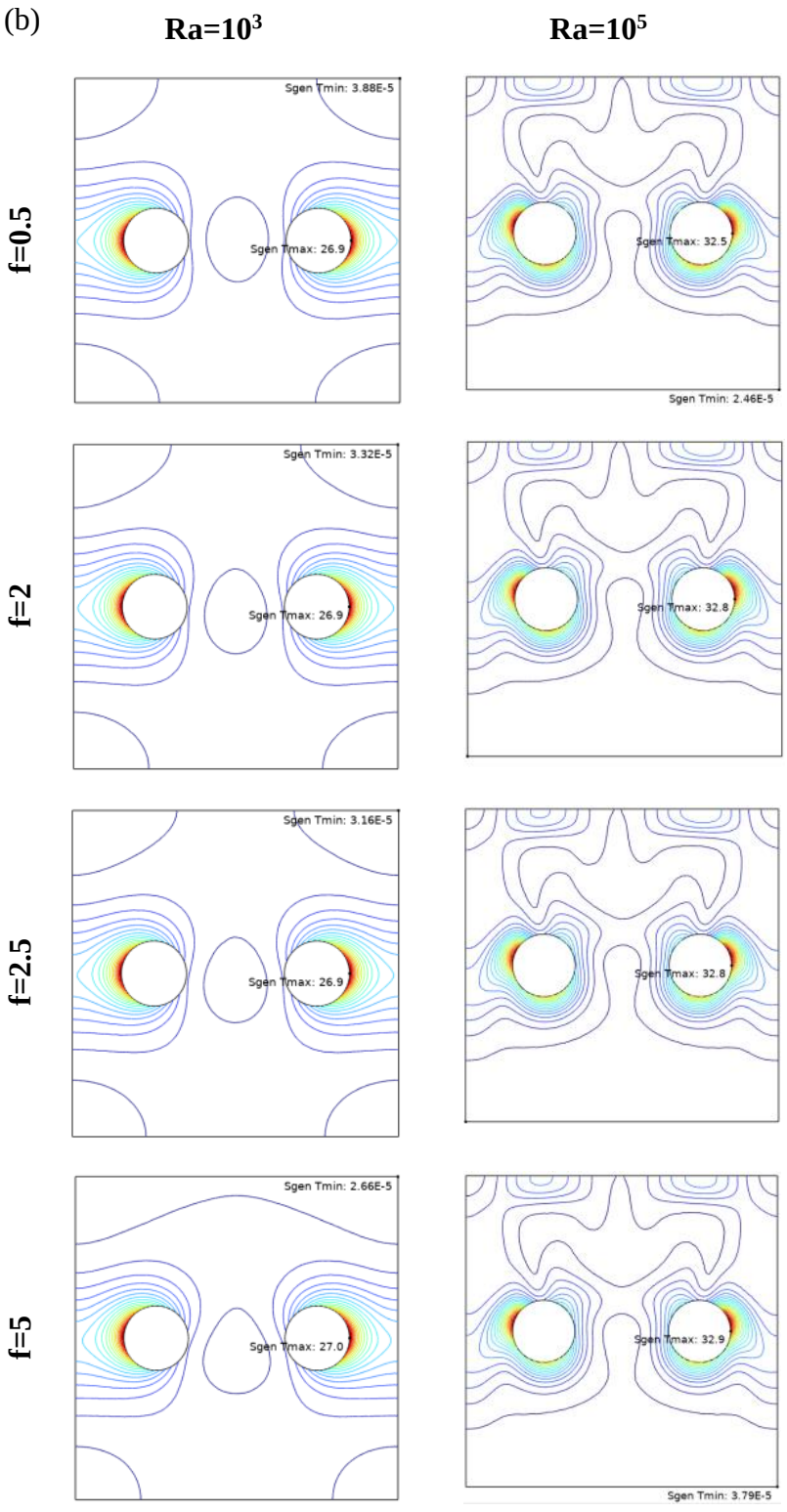
Ra=10^3
Ra=10^5
f=0.5
f=2
f=2.5
f=5
Sgen Tmin: 3.88E-5
Sgen Tmax: 26.9
Sgen Tmax: 32.5
Sgen Tmin: 2.46E-5
Sgen Tmin: 3.32E-5
Sgen Tmax: 26.9
Sgen Tmax: 32.8
Sgen Tmin: 3.16E-5
Sgen Tmax: 26.9
Sgen Tmax: 32.8
Sgen Tmin: 2.66E-5
Sgen Tmax: 27.0
Sgen Tmax: 32.9
Sgen Tmin: 3.79E-5

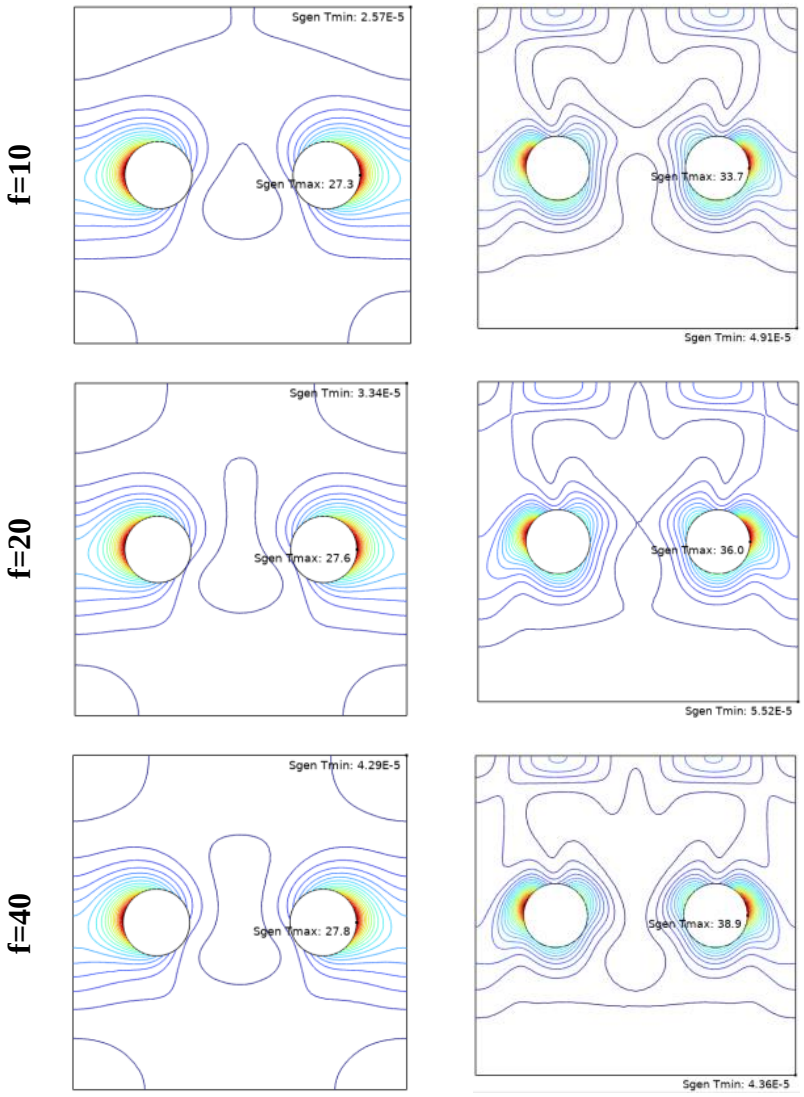

Fig. 6. The minimum and maximum entropy values and their locations at Rayleigh numbers 103, and 105. Di = 2, τ = 2, φhpn = 0.5. a) f= 2; b) A=0.1.

(a) **Ra=10^3** **Ra=10^5**

A=0

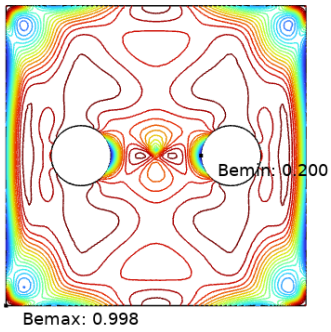

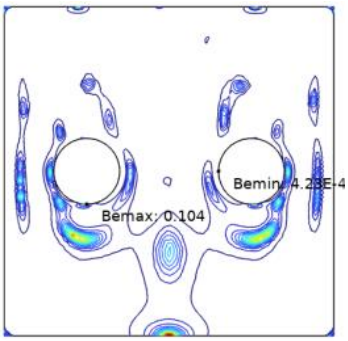

A=0.05

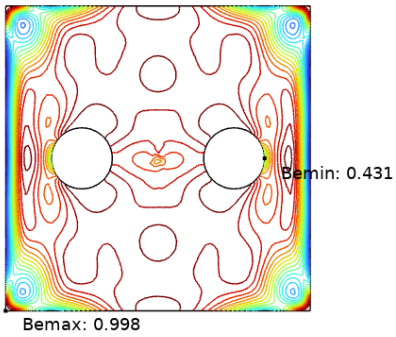

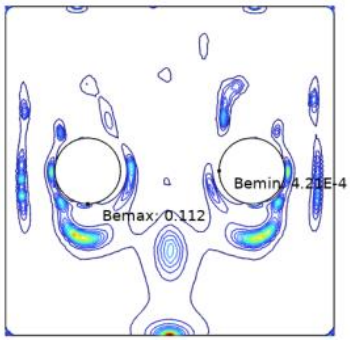

A=0.1

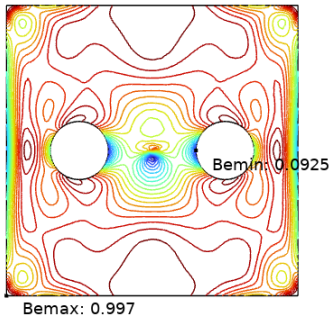

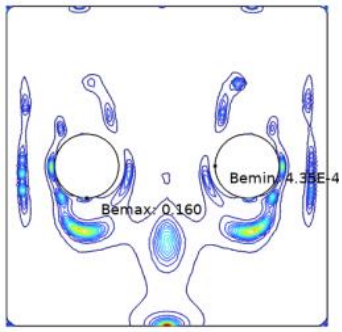

A=0.15

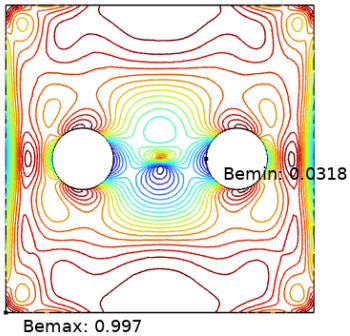

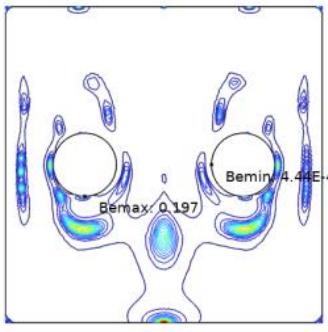

(b) **Ra=10^3** **Ra=10^5**

f=0.5

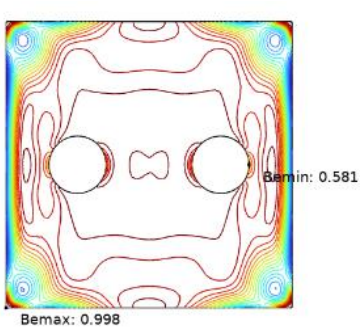

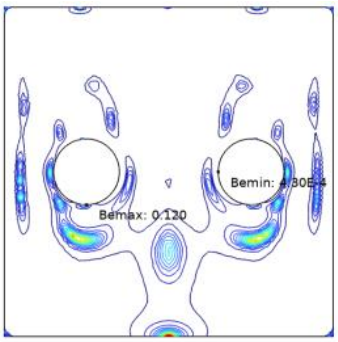

f=2

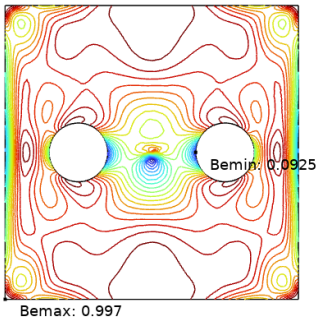

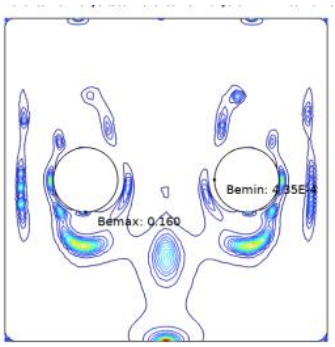

f=2.5

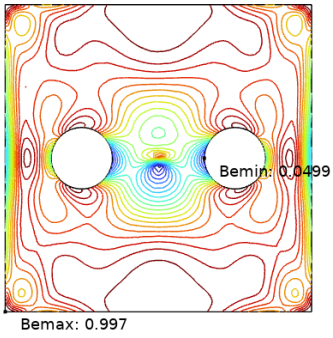

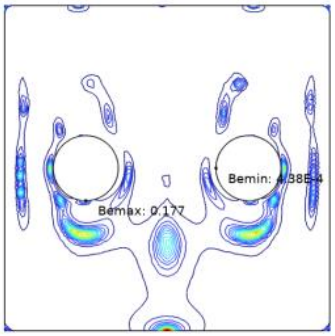

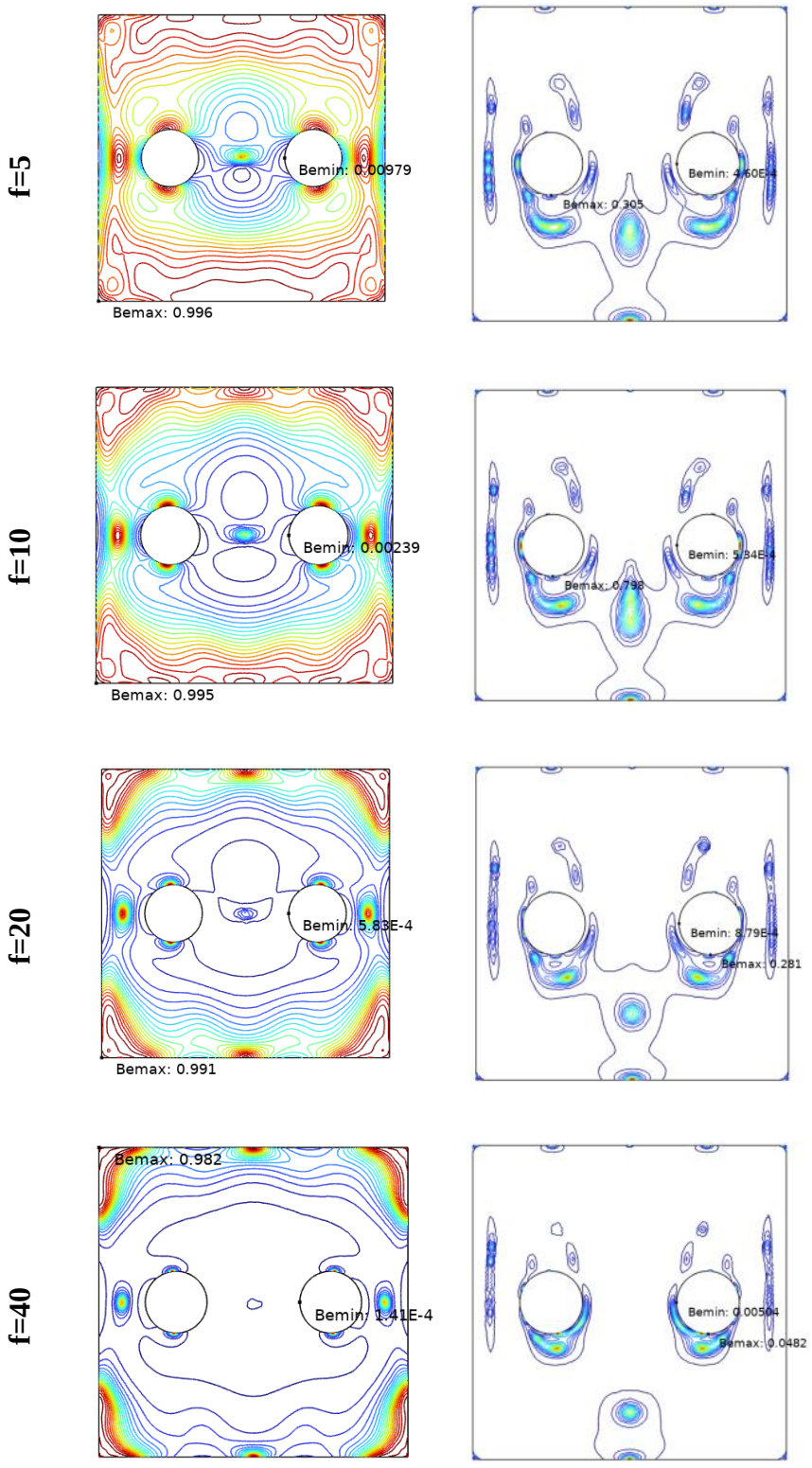

Fig. 7. Highest and lowest values of the Bejan number at Rayleigh numbers 10^3, and 10^5, Di = 2, τ = 2, φ_{hpn} = 0.5. a) f=2; b) A =0.1.

Ra 10^3

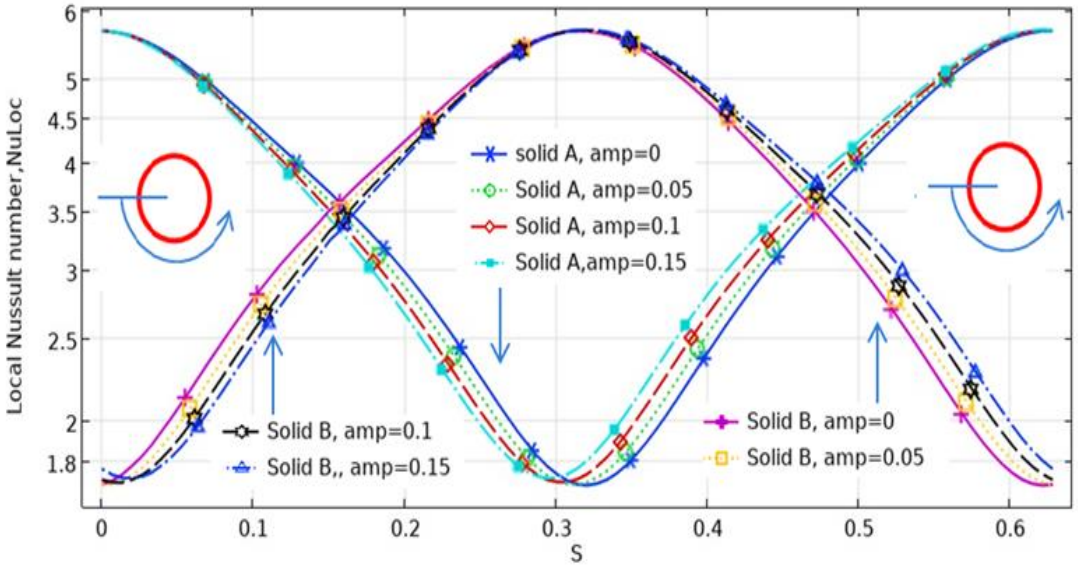

Ra 10^5

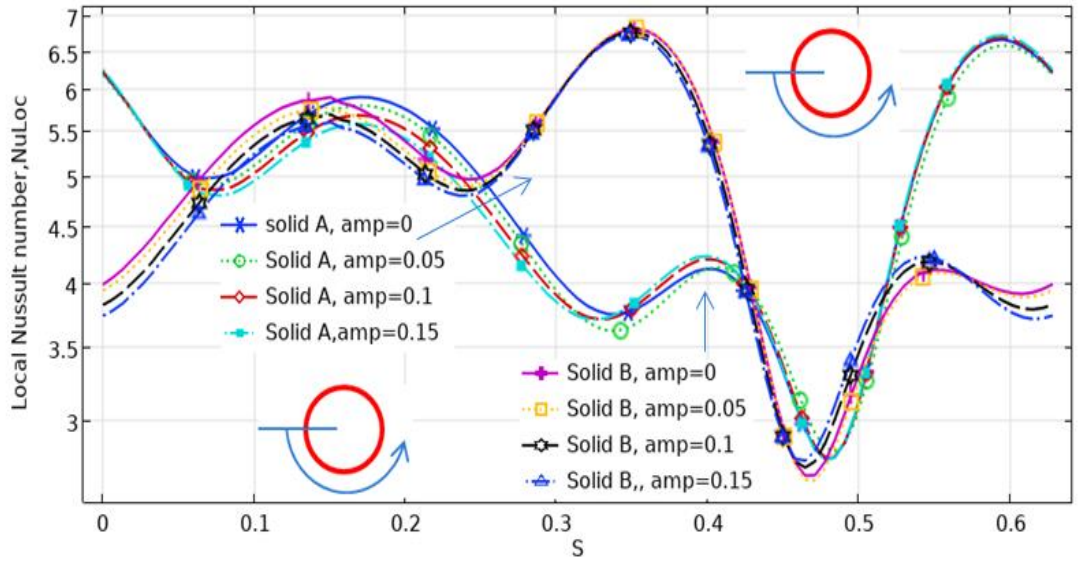

Fig. 8. Local Nusselt Number at Rayleigh numbers 10^3, 10^4, and 10^5. Di = 2, f =2, τ = 2, φ_{hpn} = 0.5.

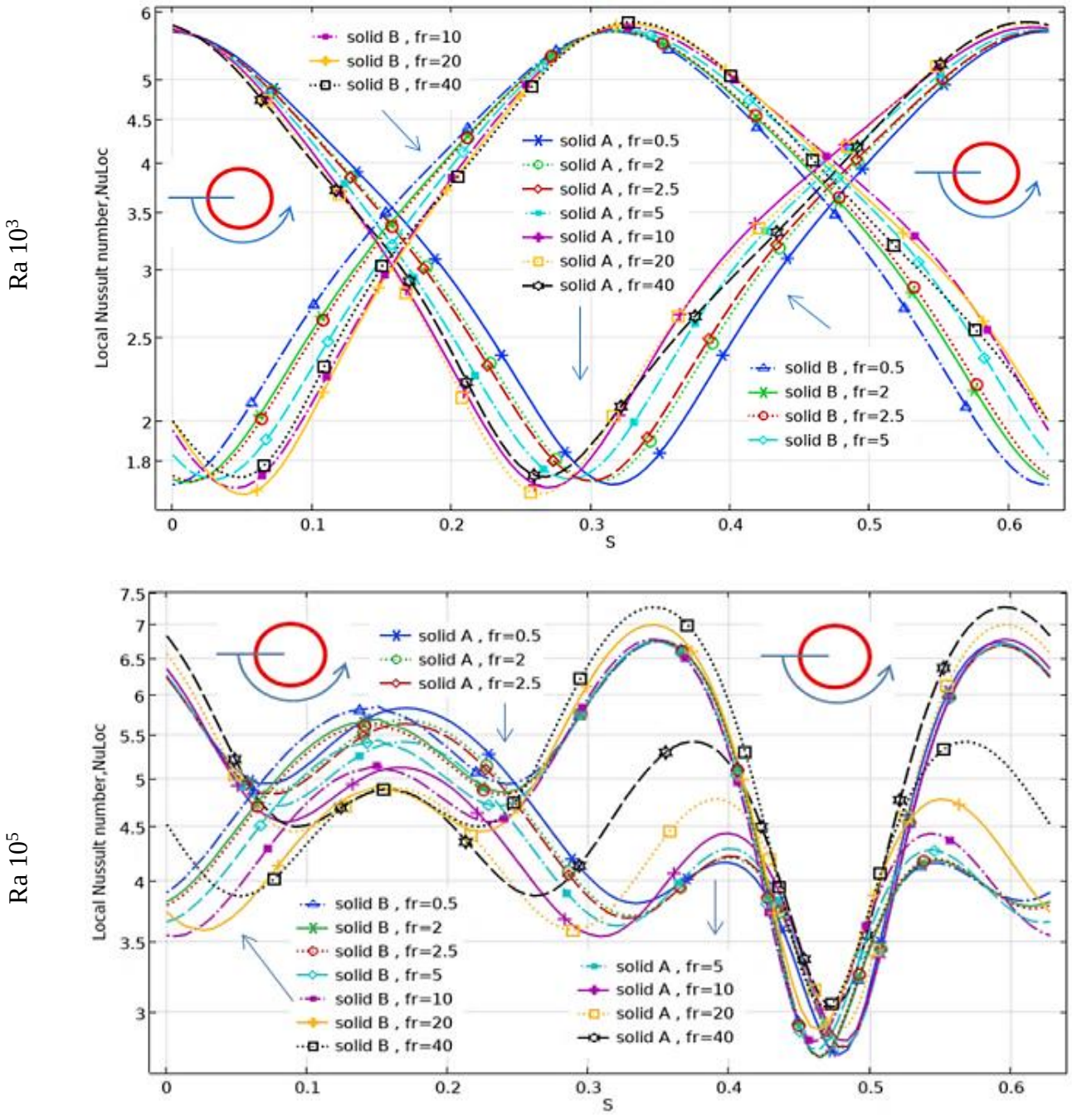

Fig. 9. Local Nusselt Number at Rayleigh numbers 10^3, 10^4, and 10^5. Di = 2, A =2, τ = 2, φ_{hpn} = 0.5.

REFERENCES

A. Abdulkadhim, K. Al-Farhany, and A. M. Abed 'Effect of Adiabatic Circular Cylinder on the Natural Convection Heat Transfer Characterizes in a Porous Enclosure' Chemical Engineering Transactions, Vol. 71, 2018. doi:10.3303/CET1871219.

A. Abdulsahib and K. Al-Farhany. 'Experimental Investigation of Mixed Convection on a Rotating Circular Cylinder in a Cavity Filled With Nanofluid and Porous Media' Al-Qadisiyah Journal for Engineering Sciences, Vol. 13, pp. 99–108, 2020. doi:10.30772/qjes. v13i2.653.

A.Kh. Kareem, H.A. Mohammed, A. K. Hussein and Shian Gao, 'Numerical investigation of mixed convection heat transfer of nanofluids in a lid-driven trapezoidal cavity' International Communications in Heat and Mass Transfer,Vol. 77, pp. 195–205, 2016. doi:10.1016/j.icheatmasstransfer.2016.08.010.

A.Rashad , A. J. Chamkha, Ismael, M. A. and T. Salah, 'Magneto hydrodynamics Natural Convection in a Triangular Cavity Filled with a Cu–Al_2O_3/Water Hybrid Nanofluid with Localized Heating from Below and Internal Heat Generation', Journal of Heat Transfer, Vol. 140, No. 7, 072502, 2018. doi: 10.1115/1.4039213.

A. S. Abedallh, O. R. Alomar and N. J. Yasin, 'Numerical and experimental investigation on mixed convection heat transfer inside cavity heated from below with reciprocating moving upper surface' International Communications in Heat and Mass Transfer, Vol. 159, Part C, 108242, 2024. doi:10.1016/j.icheatmasstransfer.2024.108242.

B. M. Al-Srayyih, A. Al-Manea, K. Saleh, A. M.Abed, Q. R. Al-Amir, H. K. Hamzah, F. H, Ali, Al-Rbaihat R. and Alahmer A. 'Simulation Investigation of the Oscillatory Motion of Two Elliptic Obstacles Located within a Quarter-Circle Cavity Filled with Cu-Al_2O_3/Water Hybrid Nanofluid' Numerical Heat Transfer, Part A: Applications, Vol. 86, No. 5, pp. 1328–1352, 2023. doi:10.1080/10407782.2023.227948.

Ch. Abdellahoum and A. Mataoui 'Effect of the Aspect Ratio on the Heat Transfer Enhancement by the Al_2O_3-H2O Nanofluid Traversing a Heated Shallow Cavity' WSEAS Transactions on Heat and Mass Transfer, Vol. 17, pp. 104–113, 2022. doi:10.37394/232012.2022.17.11.

D. Dey and S. K. Dash, 'An experimental investigation on the nanofluids in a cavity under natural convection with and without the rotary magnetic field' Heliyon, Vol. 9, Issue11, e22416, 2023. doi:10.1016/j.heliyon.2023.e22416.

Einstein A. 'Investigations on the Theory of the Brownian Movement'. Fürth R, editor; Cowper AD, translator, New York: Dover Publications; 1956.

Farhan A. I. and Ziad M. Al-Makhyoul, 'Mixed Convection of Heat Transfer around Rotating Cylinders inside Enclosure Filled with Nano Fluid', International Research Journal of Innovations in Engineering and Technology, Vol. 05, No. 10, pp. 51–64, 2021. doi:10.47001/IRJIET/2021.510010.

GH. R. Kefayati 'Effect of a Magnetic Field on Natural Convection in an Open Cavity Subjugated to Water/Alumina Nanofluid Using Lattice Boltzmann Method', International Communications in Heat and Mass Transfer, Vol. 40, pp. 67–77, 2013. doi:10.1016/j.icheatmasstransfer.2012.11.009

H.M. Elshehabey, F.M. Hady , S.E. Ahmed and R.A. Mohamed 'Numerical investigation for natural convection of a nanofluid in an inclined L-shaped cavity in the presence of an inclined magnetic field' International Communications in Heat and Mass Transfer, Vol. 57, pp. 228–382, 2014. doi: 10.1016/j.icheatmasstransfer.2014.07.004

K. Al Kalbani and M.J. Uddin 'Convective Heat Transfer of Hybrid Nanofluid Flow in a Cavity Having Vertical Wavy Walls', Iraqi Journal of Science, Vol. 66, No. 2, 2025. doi:10.24996/ijs.2025.66.2.7.

M. A. Hanafiah , A. Ghani , M. E. H. Hafidzuddin, N. MdArifin and M. N. Som 'Effect of nanoparticle shape on natural convection in hybrid nanofluid inside square cavity' Mathematical Modeling and Computing. Vol. 11, No. 4, pp. 1118–1127, 2024. doi: 10.23939/mmc2024.04.1118

Maxwell JC. A treatise on electricity and magnetism. Oxford: Clarendon Press; 1881.

M. Ghalambaz, S. M. Hashem Zadeh, A. Veismoradi, M. A. Sheremet, and I. Pop, 'Free Convection Heat Transfer and Entropy Generation in an Odd-Shaped Cavity Filled with a Cu–Al_2 O_3 Hybrid Nanofluid', Symmetry, Vol. 13, No. 1, Article 122, pp. 1–20, 2021. doi:10.3390/sym13010122.

M.H.M. Hashim, N. Md. Arifin, A. N. M. Som, N. M. Ali, A. Ab Ghani and S. J. Ali 'Natural Convection in Trapezoidal Cavity Containing Hybrid Nanofluid' Journal of Advanced Research in Micro and Nano Engineering, Vol. 13, pp. 18–30, 2023. doi:10.37934/armne.13.1.1830.

M.Ibrahim, A.S. Berrouk, T. Saeed, et al. ' based numerical analysis -Lattice Boltzmann of nanofluid natural convection in an inclined cavity subject to multiphysics fields' Scientific Reports, Vol. 12, 5514, 2022. doi:10.1038/s41598-022-09320-817.

R. Nasrin and M. Alim, 'Free Convective Flow of Nanofluid Having Two Nanoparticles Inside a Complicated Cavity', International Journal of Heat and Mass Transfer, Vol. 63, pp. 191–198, 2013. doi:10.1016/j.ijheatmasstransfer.2013.03.056.

R. Zhang, Ali Ghasemi, Azeez A. Barzinjy, Maliheh Zareei, Samir M. Hamad & Masoud Afrand 'Simulating Natural Convection and Entropy Generation of a Nanofluid in an Inclined Enclosure under an Angled Magnetic Field with a Circular Fin and Radiation Effect', Journal of Thermal Analysis and Calorimetry, Vol. 139, pp. 3803–3816, 2020. doi:10.1007/s10973-019-08729-0.

S. A. M. Mehryan, E. Izadpanahi, M. Ghalambaz and A. J. Chamkha 'Mixed convection flow caused by an oscillating cylinder in a square cavity filled with $Cu–Al_2O_3$/water hybrid nanofluid'. Journal of Thermal Analysis and Calorimetry, Vol. 137, pp. 965–982, 2019. doi:10.1007/s10973-019-08012-2.

S.M.S Murshed, K.C. Leong, and C.Yang 'Enhanced Thermal Conductivity of TiO_2 – Water Based Nanofluids', International Journal of Thermal Sciences, Vol. 44, No. 4, pp. 367–373, 2005. doi:10.1016/j.ijthermalsci.2004.12.005.

T. Tayebi and H.F. Öztop 'Entropy production during natural convection of hybrid nanofluid in an annular passage between horizontal confocal elliptic cylinders' International Journal of Mechanical Sciences, Vol. 171, 105378, 2020. doi:10.1016/j.ijmecsci.2020.105378.

T. Tayebi and S. Kheir 'Enhancement of Heat Transfer in a Cavity Filled with Cu-Water Nanofluid', Proceedings of CIMDD'2013, Université M'Hamed Bougara, Boumerdes, Algeria, Vol. 01, pp. 1–8, 2013. doi:10.13140/2.1.3451.7287.

Z.Gong, J. Ren, P. Si, L. Shi and Z. Wang 'Effects of Fluid–Structure Interaction on Natural Convection Heat Transfer in a Square Cavity Divided by Vertically Flexible Walls', Applied Thermal Engineering, Vol. 265, 125616, 2025. doi: 10.1016/j.applthermaleng.2025.125616.